Supplementary Material/Supporting Information

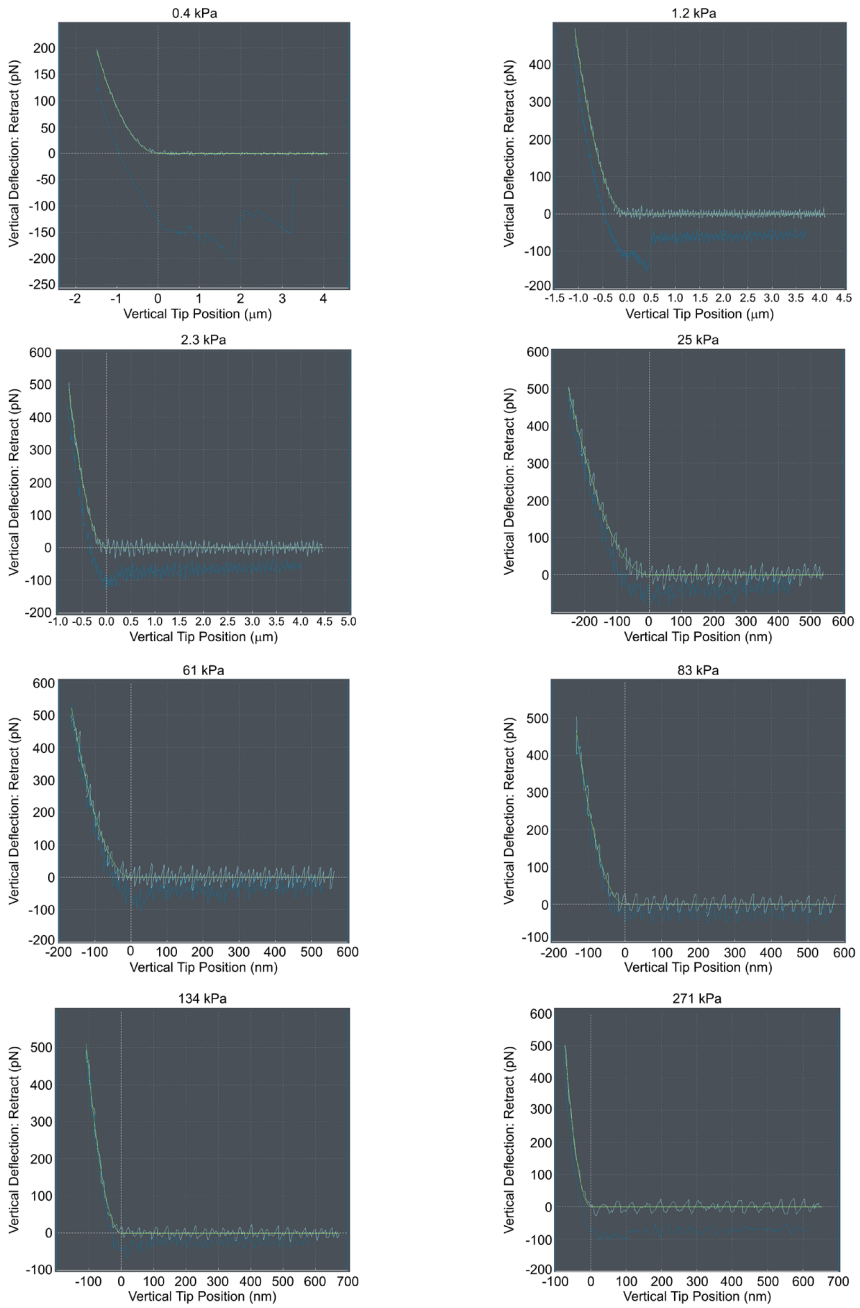

Fig. S1 | Representative force-indentation curves including the fit of the Hertzian model obtained by atomic force microscopy.

The curves for 0.4, 1.2, 2.3, 25, 61, 83, 134, and 271 kPa polyacrylamide gels are shown. Light blue: extended curve; dark blue: retract curve; green: fit curve of the Hertzian model.

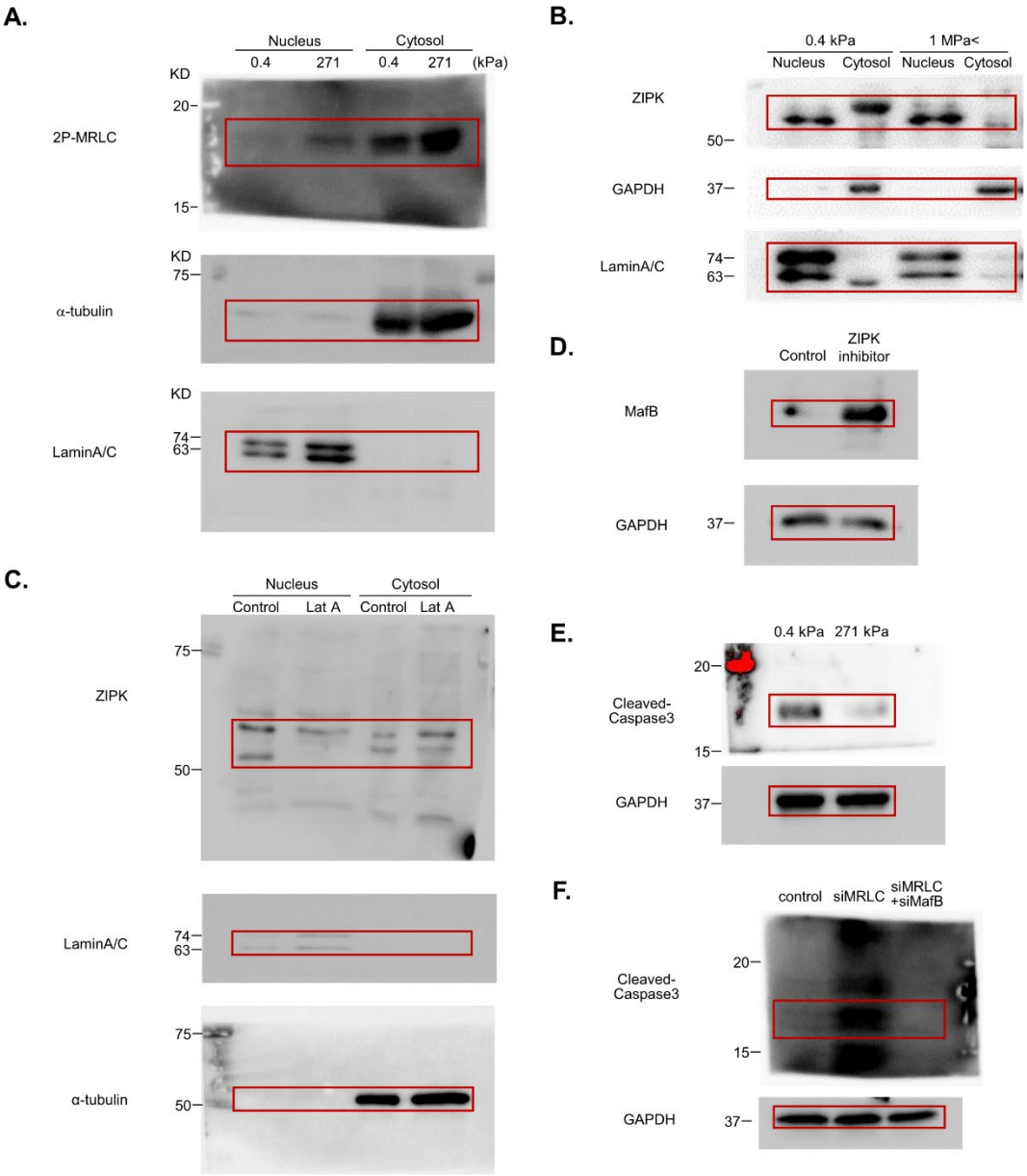

Fig. S2 | Blot transparency

(A–F) Full unedited blots for Fig. 1E (A), Fig. 2E (B), Fig. 3E (C), Fig. 4E (D), Fig. 5B (E), and Fig. 5D (F).

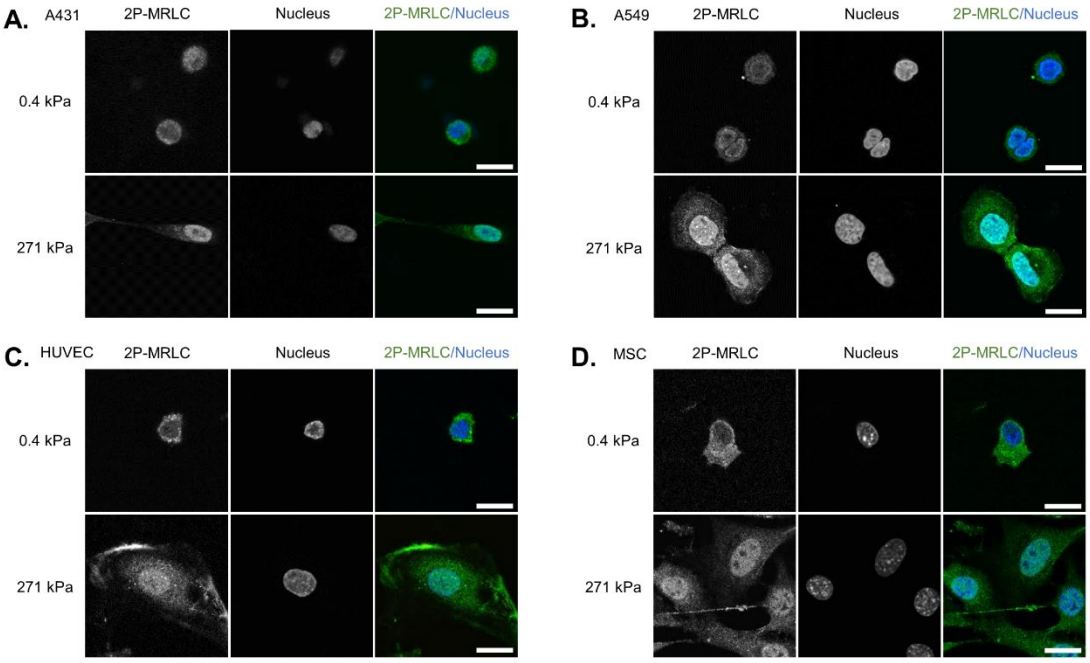

Fig. S3 | Stiff substrates promote the nuclear localization of 2P-MRLC in various cells.
(A–C) Representative immunofluorescent images of 2P-MRLC and nucleus in A431 cells (A), A549 cells (B), human umbilical vein endothelial cells (HUVECs) (C), and mesenchymal stem cells (MSCs) (D) on soft (0.4 kPa) or stiff (271 kPa) polyacrylamide hydrogel substrates. Scale bars are 20 μm.

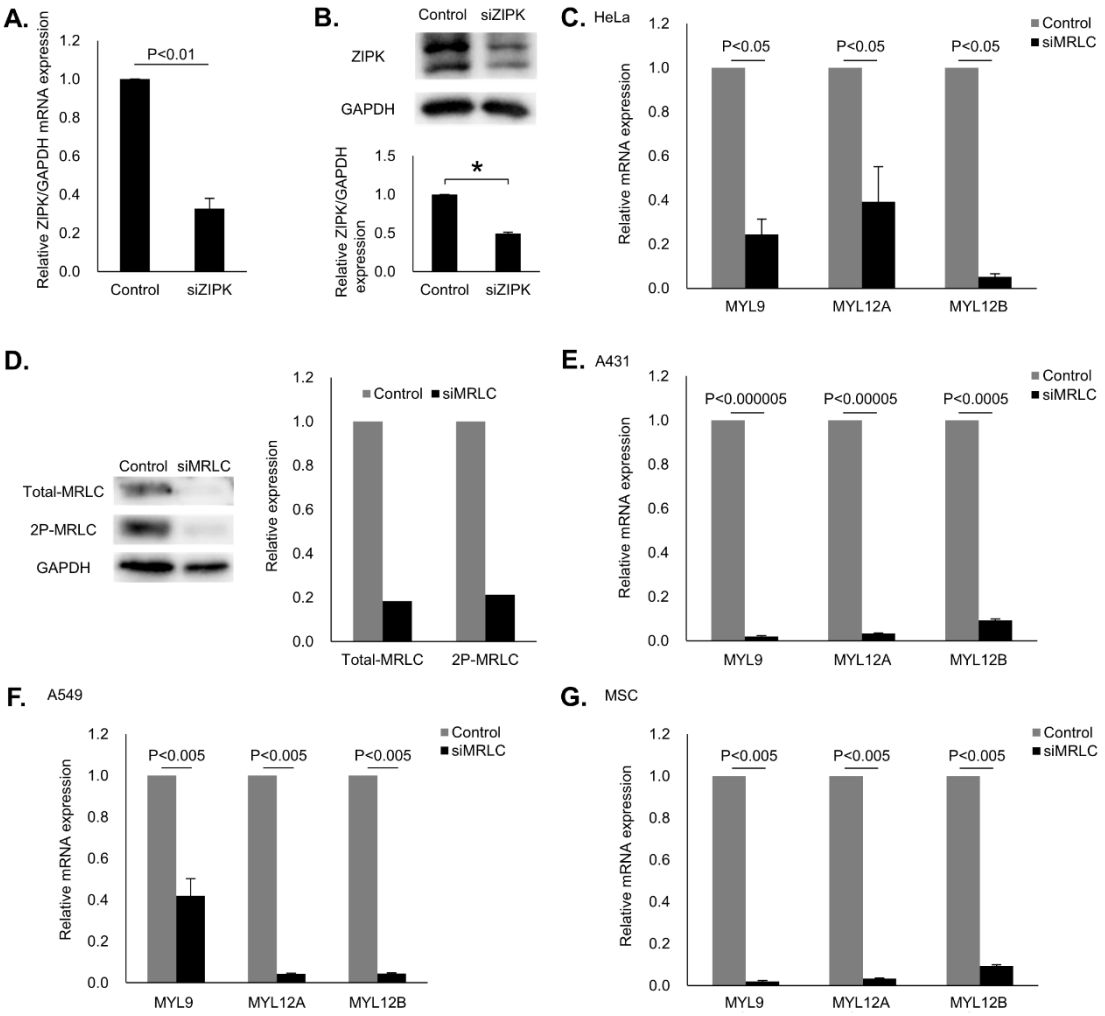

Fig. S4 | Small interfering RNA (siRNA)-mediated knockdown of ZIPK and MRLC.

(A) Relative mRNA expression of ZIPK/glyceraldehyde 3-phosphate dehydrogenase (GAPDH) determined via quantitative polymerase chain reaction (qPCR) in HeLa cells on stiff plastic substrates after transfection with the negative control of siRNA (control) or siRNA targeting ZIPK (siZIPK). (B) Western blots (left) and quantification (right) for ZIPK levels in HeLa cells on plastic substrates after transfection with the negative control of siRNA (control) or siRNA targeting ZIPK (siZIPK). n = 3 independent experiments. Bars represent the mean ± SEM. (C) Relative mRNA expression of MYL9, MYL12A, or MYL12B/GAPDH determined via qPCR in HeLa cells after transfection with the negative control of siRNA (control) or siRNA targeting MRLC (siMRLC). (D) Western blots (left) and quantification (right) of total-MRLC and 2P-MRLC levels in HeLa cells on stiff plastic substrates after transfection with the negative control siRNA (control) or siRNA targeting MRLC (siMRLC). (E–F) Relative mRNA expression of MYL9, MYL12A, or MYL12B/GAPDH determined via qPCR in A431 (E) and A549 (F) cells on stiff plastic substrates after transfection with the negative control of siRNA (control) or siRNA targeting MRLC (siMRLC). (G) Relative mRNA expression of MYL9,

MYL12A, or MYL12B/s18 determined via qPCR in MSCs on stiff plastic substrates after transfection with the negative control of siRNA (Control) or siRNA targeting MRLC (siMRLC). n = 3 experiments except (B) and (D). n = 1 experiment in (B) and (D). Bars represent the mean ± standard error of the mean (SEM). Statistical significance determined using an Welch's *t*-test except (B). *Statistical significance was determined with a 95% confidence interval in (B).

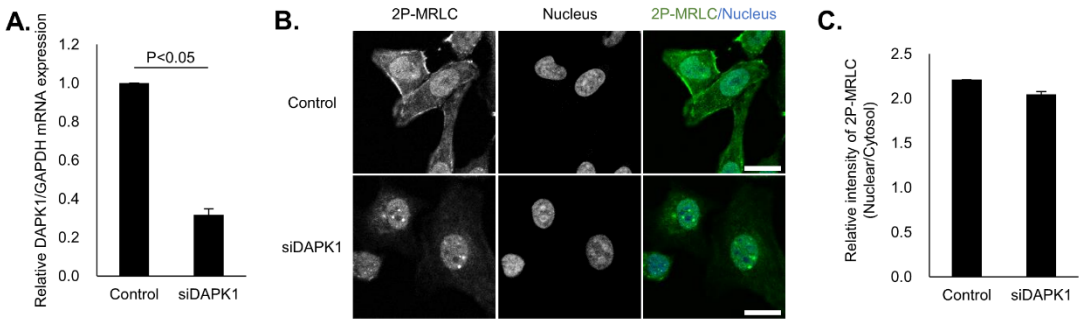

Fig. S5 | DAPK1 does not affect the nuclear localization of 2P-MRLC.

(A) Relative mRNA expression of DAPK1/GAPDH determined via qPCR in HeLa cells on stiff glass substrates coated with collagen-I after transfection with the negative control of siRNA (control) or siRNA targeting DAPK1 (siDAPK1). n = 3 experiments. Statistical significance determined using an unpaired *t*-test. Bars represent the mean ± SEM. (B) Representative immunofluorescent images of 2P-MRLC and nucleus in HeLa cells on stiff glass substrates coated with collagen-I after transfection with the negative control of siRNA (control) or siRNA targeting DAPK1 (siDAPK1). (C) Quantification of the fluorescent intensity of 2P-MRLC in the nucleus relative to the cytosol from (B). n = at least 40 cells in two independent experiments. Scale bars are 20 μm. Bars represent the mean ± SEM.

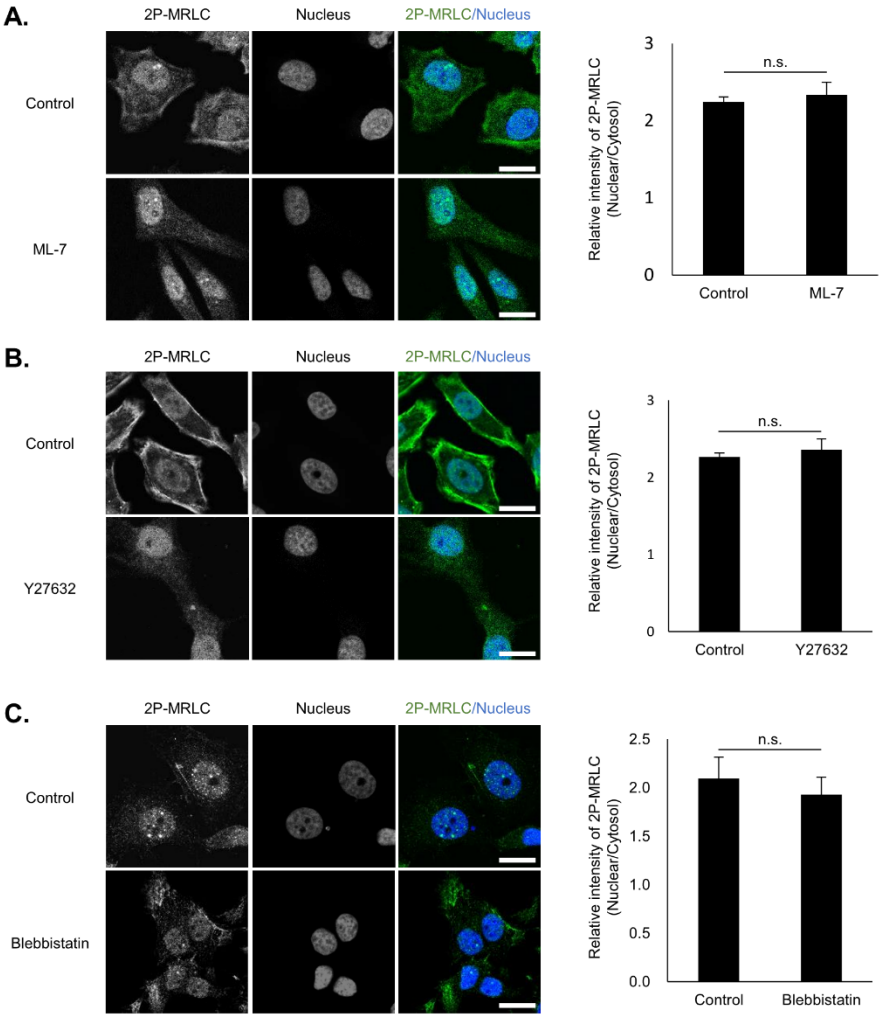

Fig. S6 | Myosin light-chain kinase (MLCK), Rho-associated protein kinase (ROCK), or myosin-II activity does not affect the nuclear localization of 2P-MRLC.

(A–C) Representative immunofluorescent images of 2P-MRLC and nucleus (left) and quantification of the fluorescent intensity of 2P-MRLC in the nucleus relative to that in the cytosol (right) in HeLa cells on stiff glass substrates coated with collagen-I after treatment with or without ML-7 (A), Y27632 (B), and blebbistatin (C). Scale bars are 20 μm. n = at least 60 cells in three independent experiments. Bars represent the mean ± SEM. Statistical significance determined using an unpaired *t*-test. n.s., not significant.

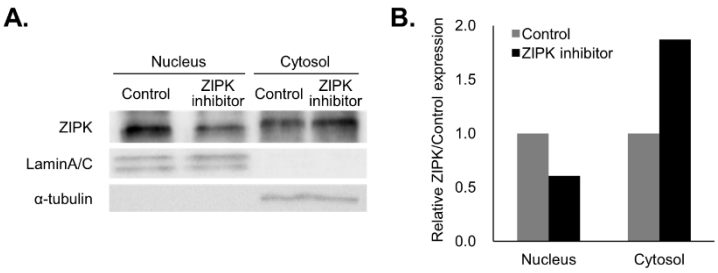

Fig. S7｜Inhibition of ZIPK suppresses its nuclear localization.

(A) Representative western blots of the nuclear and cytosolic extracts of HeLa cells on stiff plastic (>1MPa) substrates coated with collagen-I after treatment with DMSO (control) or ZIPK inhibitor using anti-ZIPK, anti-α-tubulin , and anti-LaminA/C antibodies. (B) Relative ZIPK expression of (A). Ratio of ZIPK to internal control is shown. LaminA/C and α-tubulin were used as the internal controls for nuclear and cytosolic extracts, respectively. n = 1 experiment.

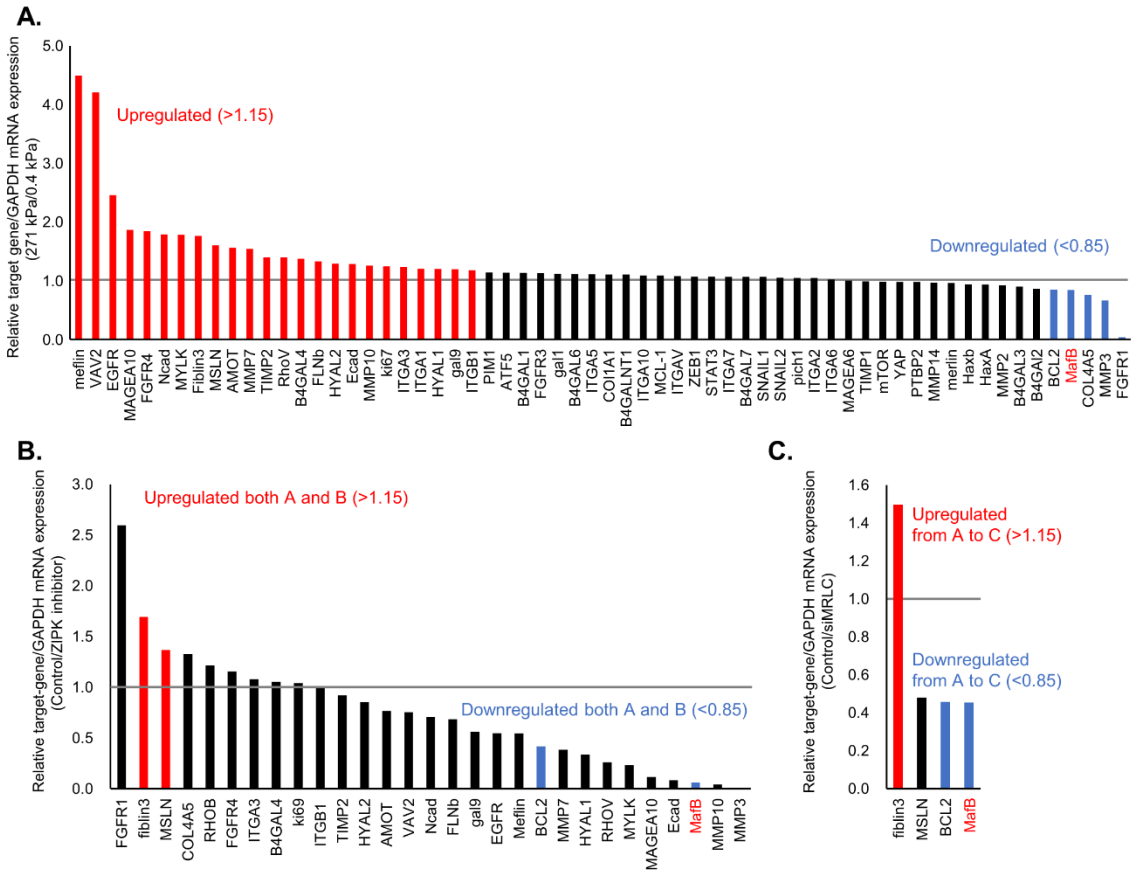

Fig S8 | First screening to determine the genes whose expression is regulated by nuclear 2P-MRLC.

(A–C) Relative mRNA expression of the target-gene/GAPDH in HeLa cells on stiff (271 kPa) relative to soft (0.4 kPa) polyacrylamide hydrogel substrates (A), on stiff plastic substrates after treatment with dimethyl sulfoxide (DMSO) (control) relative to ZIPK inhibitor (B), and on stiff plastic substrates after transfection with the negative control of siRNA (Control) relative to siRNA targeting MRLC (siMRLC) (C). n = 1 experiment.

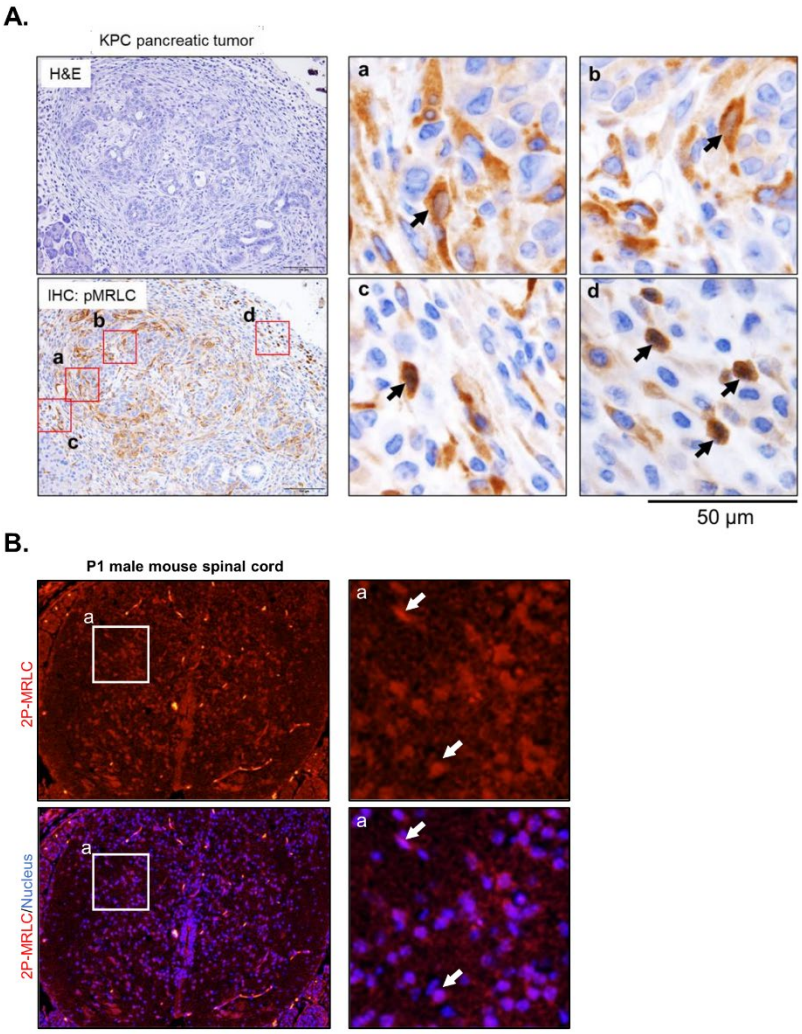

Fig. S9 | 2P-MRLC localized to the nucleus of cells that constitute pancreatic cancer or P1 male mouse spinal cord.

(A) Tissue sections from pancreatic cancer developed in the KPC model were stained with hematoxylin and eosin (H&E, left upper panel) and 2P-MRLC (left lower panel). Boxed regions (a–d) were magnified in adjacent panels. Arrows indicate the cells in which weak to moderate nuclear 2P-MRLC signals were observed. (B) Immunohistochemical staining image of 2P-MRLC in P1 male mouse spinal cord. Arrows indicate the cells in which nuclear 2P-MRLC signals were observed.

	0.4 kPa polyacrylamidogel				271 kPa polyacrylamidogel		
	Young's modurus（Pa）				Young's modurus（Pa）		
	observation1	observation2	observation3		observation1	observation2	observation3
1	671	267	502	1	231268	329984	251283
2	580	268	529	2	279207	221447	289208
3	611	263	439	3	257660	252433	251263
4	574	268	438	4	336689	271227	308161
5	633	276	382	5	312899	269021	256243
6	601	285	461	6	275581	205329	259916
7	616	268		7	300420	263960	269490
8	639	267		8	295964	258155	267851
9	642	293		9	250939	267966	265150
10	595	252		10	290666	240917	263252
11	676	290		11	278668	259150	272202
12	628	262		12	263981	254876	301057
13		261		13	344578	255106	217952
14				14	299499	263214	225290
15				15	254104	289055	263075
16				16	287384	333266	306067
17				17	274488	251046	286385
18				18	237723	216469	296650
19				19	273892	260815	259507
20				20	293726	268294	293050
21				21	280136	281202	256357
22				22	318173	260041	246022
23				23	324545	304266	338419
24				24	285231	302475	282265
25				25	287950	293541	274546
26				26	248763	246878	276934
27				27	295780	286564	330781
28				28	276019	256352	293625
29				29	267877	296078	197557
30				30	310409	262328	204092
31				31	270763	288534	270601
32				32	309633	273034	249181
33				33	317040	322436	268061
34				34	285053	323938	276660
35				35	289968	283203	281837
36				36	263589	250771	298086
37				37	243319	287612	297591
38				38	268620	284160	194276
39				39	280055	278212	238683
40				40	264054	303136	255428
41				41	223098	291964	259199
42				42	268468	309408	272817
43				43	258314	260997	241105
44				44	264616	266839	229824
45				45	233456	294010	286258
46				46	268805	333687	276079
47				47	292256	360067	253108
48				48	252526	273204	230880
49				49	278717	263494	251904
50				50	260820	275072	283750
51				51	247566	313501	206712
52				52	297129	261915	310177
53				53	248867	277744	257946
54				54	231170	257436	290873
55				55	270751	289533	240142
56				56	260453	250910	261035
57				57	286254	284574	277182
58				58	275389	293892	245182
59				59	262303	272803	258451
60				60	258893	217460	217080
61				61	256847	254262	266810
62				62	265750	260326	251651
63				63	244113	267226	257680
64				64	275701	244815	250931
Average	622	271	458		275134	274869	264232
Average of 3 observation	450				271412		
Standard deviation	176				6219		

	1.2 kPa polyacrylamidogel			2.3 kPa polyacrylamidogel			25 kPa polyacrylamidogel		
	Young's modurus（Pa）			Young's modurus（Pa）			Young's modurus（Pa）		
	observation1	observation2	observation3	observation1	observation2	observation3	observation1	observation2	observation3
1	1266	1234	1192	2304	2082	2379	25094	25790	25694
2	1255	1197	1262	2371	2113	2367	24265	25694	25780
3	1232	1209	1178	2309	2058	2303	26727	24413	25336
4	1238	1246	1146	2126	2234	2326	24451	22356	26751
5	1252	1189	1287	2316	2000	2338	23537	25836	28074
6	1259	1209	1244	2445	2069	2297	26805	25553	28644
7	1226	1235	1193	2457	2065	2331	23967	24598	26793
8	1230	1316	1173	2249	2135	2492	20526	24812	26656
9	1271	1197	1225	2441	2169	2255	21915	27189	26405
10	1252	1200	1364	2436	2207	2308	24157	26491	27750
11	1232	1213	1192	2349	2291	2527	30813	26764	25865
12	1220	1330	1162	2339	2264	2661	19602	26442	26431
13	1270	1187	1183	2480	2263	2218	20440	26713	
14	1291	1168	1172	2466	2342	2461	24372	25758	
15	1229	1206	1161	2407	2456	2722			
16	1223	1308	1169	2386	2436	2749			
Average	1247	1228	1206	2368	2199	2421	24048	25601	26682
Average of 3 observation	1227			2329			25443		
Standard deviation	20			116			1324		

	61 kPa polyacrylamidogel			83 kPa polyacrylamidogel			134 kPa polyacrylamidogel		
	Young's modurus（Pa）			Young's modurus（Pa）			Young's modurus（Pa）		
	observation1	observation2	observation3	observation1	observation2	observation3	observation1	observation2	observation3
1	63703	65464	64909	81832	73843	92066	131155	132182	140372
2	65595	63892	57912	80386	79391	86330	123964	130869	147846
3	64058	64034	65021	74731	73572	87568	146293	120081	157140
4	59764	64810	65878	77431	80661	97728	137199	119565	160753
5	65333	66265	58240	87489	74037	101888	129129	126708	131741
6	65418	60514	68843	80980	79988	90742	129219	127388	133748
7	65263	59134	64795	77926	77039	92846	156365	116083	159137
8	64025	59205	62578	75694	80669	88877	161540	125827	158791
9	60762	62197	54550	78797	79132	85110	122408	126776	120077
10	64036	55074	62253	83778	80554	94486	142108	113690	141171
11	66027	51914	60611	77360	77020	90142	129076	112099	148232
12	66184	59004	57587	80227	79920	96050	180155	124953	137112
13	55796	62633	52431	80362	73431	98399	127245	111028	117866
14	58050	55639	59007	83463	78854	85601	130763	136657	131320
15	61625	48124	57789	75671	75847	82417	124935	134832	131608
16	62107	61101	63795	81659	79945	87510	138476	123216	134432
Average	62984	59938	61012	79862	77744	91110	138127	123872	140709
Average of 3 observation	61311			82905			134236		
Standard deviation	1545			7184			9068		

Table S1 | Surface stiffness of polyacrylamide gels.

The surface stiffness of polyacrylamide gels was measured using atomic force microscopy (AFM). A maximum of 64 spots (271 kPa) or 16 spots (0.4, 1.2, 2.3, 25, 61, 83 and 134 kPa) were measured in a 1-μm^2 range per observation. Spots that could not be measured were excluded.

qPCR Primers			
Target Genes	host	Sequences（5' to 3'）	
		Forward	Reverse
GAPDH	human	TCCTGTTCGACAGTCAGCCGC	TGACCAGGCGCCCAATACGAC
MYL9	human	ACCCACCAGAAGCCAAGATGTC	GGACTGGTCAAACATTGCGAAGAC
MYL12A	human	GCCGGGACTTAACCACCAC	GTTGGATTCTTCCCCAATGAAGC
MYL12B	human	TGCCATGATGAATGAGGCCC	TCCTGAATGGTGCCTGTTGC
DAPK1	human	GCTGCAAATGATCCCACGTC	ACCGAAGGCTATGGGTTCTTC
ZIPK	human	TCTTCGAGAACAAGAC	CAGCATGATGTTTTCC
MafB	human	ACCAGCTCGTGTCCATGTC	CTGCTGGACGCGTTTATACC
s18	mouse	ACTTTTGGGCCTTCGTGTC	GCAAAGGCCCAGAGACTCAT
MafB	mouse	AGGTATAAACGCGTCCAGCAG	TGGCGAGTTTCTCGCACTTG
MYL9	mouse	TTTGGGGAGAAGCTGAACGG	TCCTCGTGGATGAAGCCTGAG
MYL12A	mouse	ACTGCGGAGTCTGGAAAGTTAG	TGGCGGTTAAATCCCTGCTC
MYL12B	mouse	TCTGGGGAAGAATCCCACTGATGC	TAATCCTCCTGGATGGTGCCTGTG

Table S2 | Primers for real-time quantitative polymerase chain reaction (qPCR) analysis.